Journal of Materials Chemistry

Cite this: *J. Mater. Chem.*, 2011, **21**, 7849

www.rsc.org/materials

HIGHLIGHT

Current trends in the optimization of low band gap polymers in bulk heterojunction photovoltaic devices

Jodi M. Szarko,[a] Jianchang Guo,[bc] Brian S. Rolczynski[ab] and Lin X. Chen*[ab]

DOI: 10.1039/c0jm04433d

Applications of low band gap polymers in solar cells have attracted intense attention due to their energetic overlap with the solar spectrum. Recently, low band gap organic photovoltaic (OPV) materials have shown an unprecedented ~8% efficiency in solar cell devices. Although the energetic alignment is crucial in the optimization of these materials, the structural and kinetic effects are also important factors in the overall device performance. Here we focus on the morphology and charge separation kinetics of several energetically similar low band gap materials. Special emphasis will be on two polymers, **PF** and **PTB**, in this report.

1. Introduction

Since the discovery of photoconducting polymers,[1,2] there has been an increasing interest in improving, understanding, and modifying the building blocks of these structures to make more efficient, low cost, durable materials for various applications.[3–13] Photoconducting polymers can be used in devices such as organic light emitting diodes (OLEDs)[14] and organic photovoltaic (OPV) cells.[15] In particular, low band gap polymers are currently extensively explored for OPV cells due to their relevance to renewable energy sources in this era of rising world energy consumption. Inexpensive "roll to roll" (R2R) methods are currently being employed as a means to make OPV production competitive costwise compared to the production of more conventional solar cell materials such as silicon.[11,16] Although many OPV polymer materials have been studied, derivatives of polythiophene, such as poly (3-hexylthiophene) (**P3HT**), are commonly used as the electron donor, while the electron acceptor is typically a molecule such as [6,6]-phenyl-C_{61}-butyric acid methyl ester (**PCBM**). In spite of their intense absorption in the visible region, **P3HT** derivatives are still not energetically optimized for light harvesting from the solar spectrum, especially in the near IR region. Therefore, much effort has been put into lowering the band gap of

[a]*Department of Chemistry, Northwestern University, 2145 Sheridan Road, EvanstonIL, 60208, USA. E-mail: l-chen@northwestern.edu*
[b]*Chemical Sciences and Engineering Division, Argonne National Laboratory, 9700 South Cass Avenue, ArgonneIL, 60439, USA*
[c]*Department of Chemistry and The James Franck Institute, The University of Chicago, 929 E 57th. Street, ChicagoIL, 60637, USA*

Jodi M. Szarko

Jodi M. Szarko received her BA from Wesleyan University and her PhD from the University of Colorado at Boulder. After working at the Helmholtz Centrum Berlin, she is currently a Postdoctoral Researcher at Northwestern University. Her main focus is on the structural and kinetic properties of organic photovoltaics.

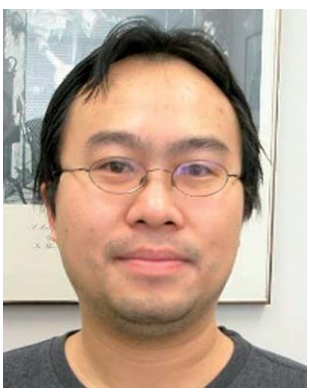

Jianchang Guo

Dr Jianchang Guo conducted his PhD, MS and BS at Emory University (USA), Dalian Institute of Chemical Physics (China), and Xiangtan University (China), respectively. He is currently a Postdoctoral Fellow in the Chemical Science Division of Oak Ridge National Laboratory, USA. Jianchang's research interests include applications of ultrafast laser spectroscopy in polymer solar cell, super-capacitors and Li-ion battery materials.

photoconducting polymers by chemical modification, such as synthesizing copolymers with alternating electron rich and electron deficient units.[17] A series of low band gap polymers synthesized by Yongye Liang and Luping Yu at the University of Chicago are such examples.[6,9,18–23] These polymers have various ring structures throughout the chain, but a common electron withdrawing thieno[3,4-*b*] thiophene unit is also incorporated into the backbone chain of all polymers in this work. The low band gap poly-thienothiophene-benzodithiophene (**PTB**) polymers have essentially the same sequence of alternating thieno[3,4-*b*] thiophene (**TT**) and benzodithiophene (**BDT**) monomer units attached with different side groups. Over ten **PTB** polymers have been reported up to date and differ by their aliphatic pendant side chains and presence of fluorine on the **TT** unit. The **PTB** polymers, when used as electron donor materials in the bulk heterojunction solar cells, truly stand out as one of the most highly efficient polymer systems in production today. In this report, the **PTB** polymers, particularly **PTB1** and **PTB7**, are compared to another low band gap polymer, **PF**, with very similar energetic properties. Although harvesting more photons from the sun may enhance the device efficiency, other factors, such as the morphology and charge separation dynamics in the bulk heterojunction (BHJ) films, also affect the overall device power conversion efficiency (PCE). We present detailed studies of **PTB** and **PF** polymer structures and properties using grazing incidence X-ray scattering (GIXS) and ultrafast transient absorption methods. We will highlight the advantages and drawbacks of polymer materials in present studies and compare them to the benchmark polymer, **P3HT**, that has been studied extensively in the past decades. We will also demonstrate three key optimization factors for the OPV device efficiency to benefit from the low band gaps in the photoconduction polymers: (1) the energy levels of the HOMO and LUMO in the polymers, (2) the morphology differences in neat and bulk heterojunction (BHJ) films and (3) the kinetics of charge transfer and charge transport in these films. It should be noted that this highlight focuses on the initial physical and photophysical properties in active conductive polymers important for solar cell optimization. For further details on the considerations of solar cell processing in devices and the complex issues regarding optimization of device processing such as R2R methods and polymer stability, the reader is directed to several other works which deal with these issues in more detail.[16,24–28]

2. Band gap energies and band level alignment in OPV devices

In general, OPV devices are comprised of five layers: (1) an indium tin oxide (ITO) anode, (2) a hole collecting layer such as PEDOT:PSS, (3) an active layer that typically comprises a blended film of a polymer donor material and a fullerene acceptor material, (4) a cathode interfacial layer such as LiF, and (5) an Al cathode.[29] Although the energetic levels of all of these layers are important in the overall device efficiency, we will mainly focus here on the energetic differences of the active layer. A schematic of the HOMO and LUMO levels of the electron donor and acceptor materials is shown in Fig. 1.[15] Two important parameters in Fig. 1 are intimately connected to the overall device efficiency: (1) the energy difference between the HOMO level of the donor and the LUMO level of the acceptor and (2) the energetic overlap with the solar spectrum. In addition, the relative positions of the LUMO levels of both the donor and the acceptor moieties will determine the driving force of the charge separation and therefore the overall device performance. Therefore, a delicate balance is present between the low band gap of the material and the driving force for the charge separation in order to reach an optimal open circuit voltage V_{OC}, and hence the optimal efficiency in the OPV device.[30]

The structures of four polymers, **P3HT**, **PF**, **PTB7**, and **PTTD**, along with their corresponding absorption spectra are shown in Fig. 2. **P3HT** is often used as a benchmark material to which novel polymer materials are compared. The three low band gap polymers, **PF**, **PTB7**, and **PTTD**, all have a common thieno[3,4-*b*] thiophene (**TT**) unit

Brian S. Rolczynski

Brian S. Rolczynski received his BA in English and his BS in Chemistry at the University of Washington. He is currently a graduate student at Northwestern University studying the spectral and dynamic properties of systematically altered low band gap copolymers.

Lin X. Chen

Lin X. Chen is Senior Chemist in Argonne National Laboratory and Professor of Chemistry at Northwestern University. Her research is currently focused on ultrafast transient molecular structural studies in solar energy conversion processes and structures–dynamics–efficiency correlations in organic photovoltaic materials using ultrafast laser and X-ray spectroscopies and X-ray structural characterization. She received her BSc and PhD degrees from Peking University in China and the University of Chicago, respectively. Her group website is at http://chemgroups.northwestern.edu/chen_group/.

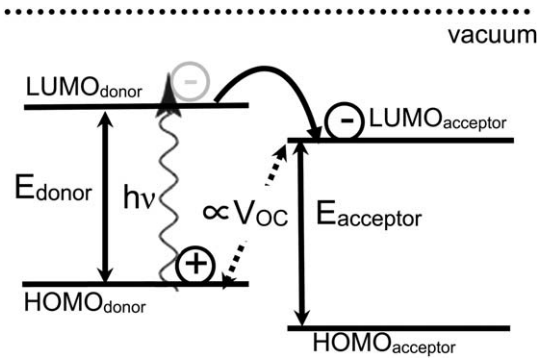

Fig. 1 Band gap alignment schematic. From ref. 15.

incorporated into the polymer backbone. **Poly-TT** has been synthesized and has a band gap as low as 0.85 V, which is too low for any effective charge transfer in typical bulk heterojunction (BHJ) devices because its LUMO level lies far below the LUMO level of **PCBM**. Therefore, the **TT** unit was connected sequentially with (a) different stoichiometry ratios of thiophene (**T**) units, or (b) benzodithiophene (**BDT**) units to slightly increase the band gap for OPV applications. The three low band gap polymers were also fluorinated to further lower the HOMO position and therefore increase the open circuit voltage of the polymer materials.

Polymer optical band gaps are typically determined by taking the tangent crossing of the low energy side of the electronic absorption spectrum. The band gap of **P3HT** is 1.9 eV.[31] The integrated photon flux using this band gap is 42% (Fig. 2, top).[8] In contrast, **PTTD** has a band gap of 1.2 eV with an integrated photon flux of 80%.[19,22] The band gap of both **PF** and **PTB7** is ~1.6 eV, which corresponds to an integrated photon flux of 58%.[11,12] The corresponding solar cell parameters, including the cell efficiencies, are shown in Table 1. **PTB7** shows the highest solar cell efficiency while **PTTD** exhibits the poorest device parameters. The theoretical solar cell efficiency maxima with respect to both the donor band gap and the donor LUMO energy levels are shown in Fig. 3, which was adapted from previous reports.[32] Using this relationship, the optimal band gap for the device efficiency is 1.5 eV. The energetic alignment and the corresponding theoretical efficiencies for the polymers **P3HT**,[33] **PF**,[18] **PTB7**,[9] **PTB1**,[21] and **PTTD**[19] are also depicted in this figure. **PTTD** has the lowest energetic band gap at 1.2 eV, but its LUMO level is only 0.2 eV above that of the **PCBM**, which provides an insufficient driving force for the exciton splitting into an electron–hole pair.[30] The resulting power conversion efficiency results in a device power conversion efficiency (PCE) of 0.73%. The highest theoretical PCE based on the band gap and the relative band level alignment of the donor and acceptor materials is roughly 8–10% for the **PF** and various **PTB** polymers. However, the maximum PCE obtained for solar cell devices fabricated with the **PF:PC$_{60}$BM** BHJ films is only 2.4%.[18] In contrast, the maximum PCE recorded for **PTB7:PC$_{71}$BM** is over 7.4%.[9] The open circuit voltage (V_{OC}) for **PF** BHJ solar cells is 0.59 V while the open circuit voltage for **PTB7** BHJ devices is 0.76 V. This accounts for an overall ~30% increase in the device PCE for the **PTB** BHJ devices. Once again, **PTB7** differs from **PTB1** only in the pendant aliphatic chains and the addition of a fluorine atom on the **TT** units. The structures of **PTB1** and **PTB7** are shown in Fig. 3b. It has been reported previously that **PTB1** devices have a V_{OC} of 0.58 V and PCE of 4.8% when using **PC$_{61}$BM** as the acceptor material.[21] When comparing the energetics of the **PTB1** and **PF** polymers, the band level alignments of the HOMO and LUMO levels are nearly identical. Nevertheless, the **PTB1** based solar cells show a 200% increase in the device PCE compared to that of the **PF** devices. The use of **PC$_{71}$BM** has also increased the PCE of devices made from many low band gap polymers, including **PTB1** and **PTB7**.[9,21] So far, the highest PCE reported for the **PTB** polymer photovoltaics is from the device using **PC$_{71}$BM** as the acceptor material. Previous studies on the **PTB** series have shown that **PC$_{71}$BM** increases the overall PCE by 15–20%.[21] Considering the increase in the open circuit voltage and the enhanced performance due to the use of **PC$_{71}$BM** in the **PTB7** devices, the **PTB7** device should show a 50% increase in the solar cell efficiency assuming both cells are optimized. In reality, the **PTB7** devices show a 300% increase in the overall efficiency compared to the **PF** devices. Furthermore, the hole mobility of the **PTB** neat polymers shows a two to three fold increase over the neat **PF** polymers, which indicates that the transport properties of these materials are also favorable. The overall comparison of both **PTB1** and **PTB7** to **PF** suggests that other factors of the active layer besides the energetics, such as morphology and charge transport, also cause the efficiencies of the **PTB** polymer devices to increase by about a factor of two compared to the **PF** devices.

The **P3HT** and **PF** film absorption spectra (Fig. 2) display sizable red shifts compared to the solution spectra. In contrast, only slight differences are shown between the solution and thin film spectra for **PTB7** and **PTTD**. The red shifts in the **P3HT** and **PF** film spectra are attributed to the planarization of the polymer backbone chain, resulting in a longer conjugation length of the polymer chain in films.[18,34] In solution, the adjacent thiophene rings along the polymer backbone are more likely to twist relative to each other, causing a more twisted polymer backbone with a shorter conjugation length. In contrast, the **PTB** and **PTTD** polymers have more fused rings along the backbone chain, which increases the quinoidal character of these species. Therefore, there is an increase in the electron density or the effective bond order on the C–C bonds connecting the aromatic rings, which adds constraints of the twists between the adjacent aromatic rings, and hence flattens the molecules. Compared to the already rather planar chain conformation in solution, very little further flattening of the polymer chains upon the film formation occurs, and thus very little red shift in the absorption spectra of the **PTB** and **PTTD** films is observed compared to those of the solutions. Future works will also probe the

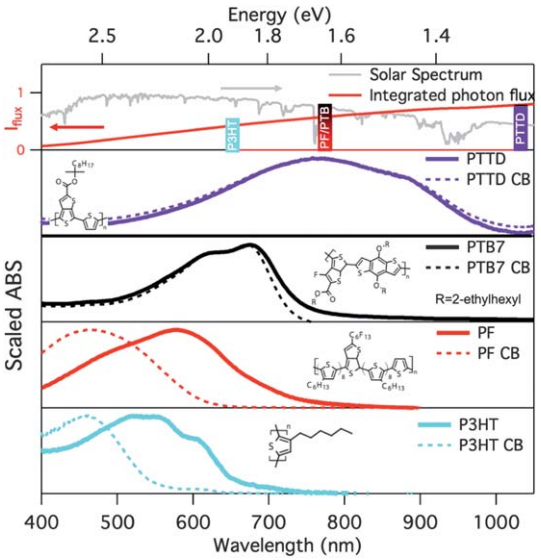

Fig. 2 Top panel: The solar absorption AM 1.5 spectrum and the corresponding integrated photon flux taken by integrating this graph. Adapted from ref. 17. Lower panels: The spectra and structures of the **PTTD**, **PTB7**, **PF**, and **P3HT** polymers in films and chlorobenzene (CB) solutions. Adapted from ref. 18–20.

effects of aggregates in solution of the **PTB** polymers.

3. Morphology differences in PF and the PTB series polymers

Using the grazing incidence X-ray scattering (GIXS) techniques, the polymer and BHJ film morphology can be investigated on different spatial scales, from molecular packing to the domain sizes and arrangements. The GIXS images for the pristine **PF** and **PTB1** films are shown in Fig. 4[18,35] and provide the scattering profiles for **PF** in the q = 0.14–1.0 Å^{-1} region (Fig. 4a) and the **PTB1** in the q = 0.15–1.9 Å^{-1} region (Fig. 4b), respectively. The domain spacing was obtained by the relationship $d = 2\pi/q$. The **PF** film structure has a morphology similar to that of **P3HT** films, which have been studied in great detail by various groups.[36–42] The ring-like structures at q = 0.39 Å^{-1} are attributed to the interatomic d-spacing (100) in the films. This spacing is determined by the width of the polymer with extended alkyl side chains on the individual thiophene units.[43,44] An enhancement of the scattering peak in the z direction is observed, which indicates that the alkyl chains attached onto the polymer backbones tend to orient perpendicular to the sample surface. Although it is not shown, the polymer backbone π–π stacking peak at $q \approx$ 1.7 Å^{-1} has also been observed in the y direction, which further indicates that the polymer backbone chain lies perpendicular to the sample surface. This morphology is typical of a polythiophene polymer material with a low molecular weight and high regioregularity. The higher order peaks are observed in **PF** films, but they are less distinct than those observed in **P3HT**. This could be due to possible irregularities introduced by the central **TT** unit on the **PF** backbone chain. This moiety can be considered as a regular quasi-defect site within the backbone chain of the material.[43] The spacing of the alkyl chain is not uniform in this region, which will hinder film uniformity. It is also important to note that the overall efficiency of **PF** was recorded as 2.38%. The efficiency of **P3HT**, when fabricated under similar conditions, was actually lower (~1.4%).[18] Over the past several decades, extensive studies on **P3HT** have increased the overall efficiency in solar cell device from less than 0.01% initially[45] to over 6%.[46,47] Compared to this benchmark material, the low band gap polymers currently under investigation are still in their infancy. Many of the improvements in the **P3HT** devices have been made in improving the morphology of the films. Since **PF** is structurally similar to **P3HT**, the similar improvements would likely enhance the solar cell performance of these materials, but the presence of this quasi-defect state could lead to a slightly different optimized morphology for the **PF** OPV devices.

The GIXS images for **PTB1** (Fig. 4b) are remarkably different from the images obtained for **PF**. The most striking feature is the anisotropic peak at q = 1.71 Å^{-1} in the z direction (Fig. 4b). This peak is attributed to the π–π stacking feature, which indicates that the polymer backbone chain lies parallel to the sample surface. This orientation is more favorable for OPV device performance. It has been shown previously that the hole transport in polymer devices is dominated by the inter-chain π–π interactions of the polymer backbone chain.[44] The relative increase in the hole mobility of the **PTB** polymers (as shown in Table 1) is partially attributed to this favorable orientation. In polymers such as **P3HT** or **PF**, the hole has to travel both intra-chain (through the backbone) and inter-chain (through the π–π interaction) pathways. In the **PTB** polymers, the hole travels predominantly through the inter-chain pathways because the π–π stacking is perpendicular to the electrode surface, so the polymer is aligned to exhibit the shortest inter-chain pathways for the hole transport. Moreover, the conjugated polymer backbone plane in this packing morphology would have an optimal interaction with the collecting anode material, hence maximizing

Table 1 The device parameters of **PTTD**, **PF**, **P3HT**, and **PTB7**. (Compiled from ref. 9–11 and 21)

	V_{oc}/V	J_{sc}/A cm^{-2}	FF	PCE (%)	μ/cm^2 V
PTTD	0.408	4.8	0.37	0.73	1.50×10^{-4}
PF	0.59	10.22	0.40	2.4	1.90×10^{-4}
P3HT	0.63	9.5	0.68	5.0	3.30×10^{-4}
PTB1	0.58	12.5	0.65	4.8	4.50×10^{-4}
PTB7[a]	0.74	14.5	0.69	7.4	5.80×10^{-4}

[a] The **PTB7** polymer devices were fabricated with **$PC_{71}BM$** while all other devices were fabricated with **$PC_{61}BM$**.

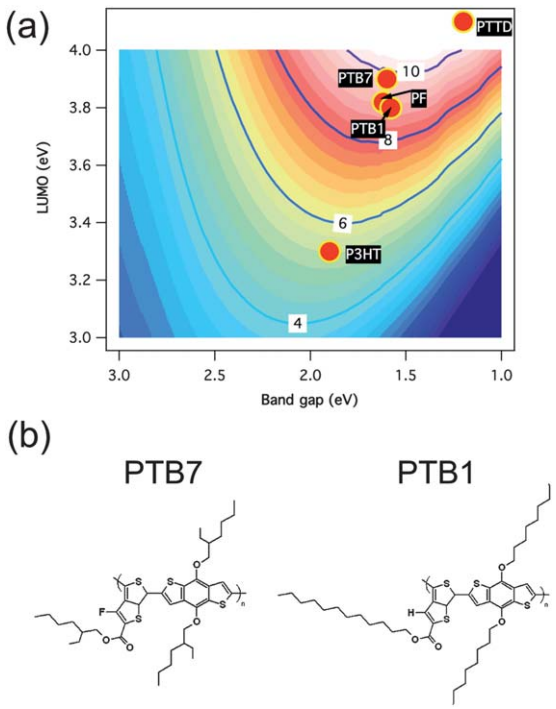

Fig. 3 (a) Contour plot showing the calculated energy-conversion efficiency (contour lines and colors) *vs.* the band gap and the LUMO level of the donor polymer. Adapted from ref. 32. (b) The chemical structures of **PTB1** and **PTB7**.

the charge transport across the active layer and surface layer interface. There is also a peak observed at $q = 0.23$ Å^{-1}, which is attributed to the (100) *d*-spacing of the polymer material. No higher order peaks are observed for this domain, which also contrasts the results obtained for the **PF** polymer. This finding indicates that the **PTB** films are less ordered. The (100) *d*-spacing is also much larger for the **PTB** polymers compared to **PF** or **P3HT** even though the alkyl side chains are similar in length, indicating that the **PTB** side chains do not intertwine in the films.

There have been many extensive and dedicated studies devoted to determining the optimal morphology of **P3HT:PCBM** films for OPV devices.[48,49] For these composite materials, it has been determined that the optimal film morphology will have the donor and acceptor domain sizes of ~10–20 nm that are connected by strands of amorphous polymer and fullerene materials.[50] Because the crystallinity for the **PTB:PCBM** films is much lower, the domain sizes are smaller and the donor:acceptor interface area is larger, the excitons do not need to travel far to the sites of the charge separation. However, the question still remains why a smaller domain size would be favorable in **PTB** polymers while other polymers must maintain some crystallinity for optimal device performance. The perpendicular polymer backbone π–π stacking orientation to the electrode surface for the **PTB** polymers could explain this discrepancy. Since the additional hole pathways can be established in a shortest pathway through the π–π stacks mentioned above in the **PTB:PCBM** films, the holes do not have to travel along a planar polymer backbone that is only enforced by a long range order in large crystalline domains. Hence, the crystallinity is not as crucial in the **PTB** films. The **PTB** films also have a higher probability to form smaller interpenetrating networks in the blended films, which would further enhance the separation and transport mechanisms in the film materials. In future works, we will also investigate the nature of the electron diffusion in a copolymer material such as the **PTB** polymers *vs.* homocyclic polymers like **P3HT**.

Although very large differences were observed in **PTB1** and **PF**, there can also be large discrepancies in the device PCE due to very small morphological differences. Recently, we have investigated morphological differences in the seven **PTB** polymers reported to date with the emphasis on the π–π stacking region.[51] These polymers have also been incorporated into OPV devices using two different acceptor materials, namely **$PC_{61}BM$** and **$PC_{71}BM$**, and in the presence or absence of an additive, 1,8-diiodooctane (DIO), in the spin casting solutions. The different kinds of **PTB** polymers synthesized and characterized, along with their device parameters, are shown in Table 2. From the results obtained here, we can see that there is a large range of PCE within the **PTB** series. The scattering profiles that represent the π–π stacking distance for the seven **PTB** polymers are shown in Fig. 5. We have discovered that the π–π stacking distance is determined almost entirely on the alkyl chain on the **BDT** unit while the efficiency dependence is determined mainly by the alkyl chain on the **TT** unit. The effects of fluorination of the **TT** units were also observed and will be discussed in future works. Even the polymer with the lowest efficiency, **PTB6**, which has a large branched group on the **TT** moiety, shows π–π stacking interaction and hence has some crystallinity in the material. Therefore, there is a delicate interplay of the morphological optimization of these materials. It is interesting to note that the **PTB** polymers have already achieved efficiencies very close to their theoretical maximum without much optimization of the production parameters. It has been shown that by using **$PC_{71}BM$** and by adding a small amount of 1,8-diiodooctane (DIO) to the casting solution will further increase the overall device PCE. If the solar cell devices do not need to undergo costly annealing procedures in order to maximize the overall efficiency, then the cost of production is greatly reduced, which makes the **PTB** polymers even more attractive for solar cell devices.

The GIXS images in the region $q \approx 0.01$–0.15 Å^{-1} were also investigated in order to reveal the long-range domain order in the BHJ films. The horizontal line profiles of the scattering images of the **PF** and **PF:PCBM** samples are shown in Fig. 6a while the scattering profiles of **PTB3**, **PTB6**, and **P3HT** are shown in Fig. 6b. The pristine films for both **PF** and **PTB1** show a linear relationship in logarithm of the scattering intensity *vs.*

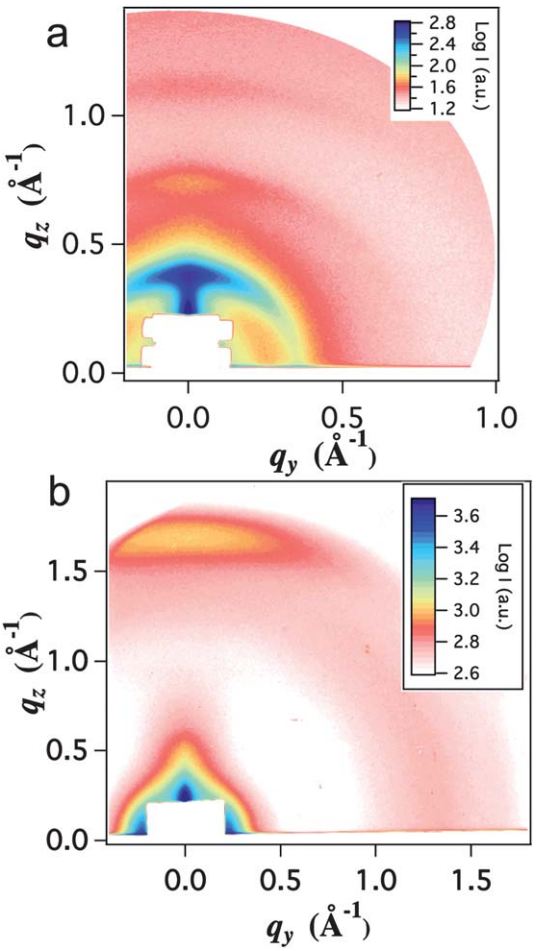

Fig. 4 The GIWAXS images for (a) **PF** and (b) **PTB1**. Adapted from ref. 18 and 35, respectively.

logarithm of the q factor, indicating the absence of distinct domains in this region. The d-spacing of 6.45 nm seen in the **PF** scattering plot is comparable to the segment length of the repeating **TT** units along the polymer chain. The **PF** or **P3HT** polymers, when blended with **PCBM**, show a distinct bend or "Guinier knee" in this region, indicating that domains of ~5–10 nm in size are present. In the **PTB** films, there is no indication of these domains. These results, along with the SEM images reported previously for blended **PTB** films,[21] indicate that these films have a bi-continuous fibrous network of polymer and fullerene materials roughly 1 nm in size.

To summarize, the grazing incidence results show that the **PTB** polymer has a favorable blended film morphology in two respects: (1) the orientation of the polymer backbone chain, which is favorable for charge transport in OPV devices and (2) the low crystallinity and nanofibrous nature of the polymer material, which increases the donor:acceptor interface area and therefore further facilitates charge separation in the material devices.

4. Exciton and charge separation dynamics in the low band gap polymer materials

The dynamics of fundamental electronic processes, such as exciton generation (EG), charge separation (CS), and charge recombination (CR) in OPV materials, are crucial for generating sufficient numbers of charge carriers for electron transport, and, ultimately, efficient photocurrent generation. These dynamic processes take place on the time scale of femtoseconds and longer, and hence can be probed by monitoring the optical signatures of transient species using ultrafast transient absorption/emission spectroscopy. The rate constants of the fundamental processes from the ultrafast spectroscopic measurements provide insight into optimization of solar cell efficiencies through energy levels and structures of polymer materials. The results from these studies, combined with the structural information obtained with

Table 2 The device parameters for 13 **PTB:PCBM** OPV devices. The preparation parameters are indicated in the second column. From ref. 51

Polymer	**PCBM**/additive	V_{OC}/V	J_{SC}/A cm^{-2}	FF (%)	PCE (%)
PTB1	**$PC_{61}BM$**/no DIO	0.58	12.5	65.4	4.76
	$PC_{71}BM$/no DIO	0.56	15.6	63.3	5.6
PTB2	**$PC_{61}BM$**/no DIO	0.60	12.8	66.3	5.10
PTB3	**$PC_{61}BM$**/no DIO	0.74	13.1	56.8	5.53
	$PC_{61}BM$/DIO	0.72	13.9	58.5	5.85
PTB4	**$PC_{61}BM$**/no DIO	0.76	9.2	44.5	3.1
	$PC_{61}BM$/DIO	0.73	13.0	61.4	6.1
	$PC_{71}BM$/DIO	0.70	15.5	64.6	7.1
PTB5	**$PC_{61}BM$**/no DIO	0.68	10.3	43.1	3.02
	$PC_{61}BM$/DIO	0.66	10.7	58.0	4.1
PTB6	**$PC_{61}BM$**/no DIO	0.62	7.7	47.0	2.26
PTB7	**$PC_{71}BM$**/no DIO	0.76	13.58	54.51	5.74
	$PC_{71}BM$/DIO	0.74	14.5	68.97	7.4

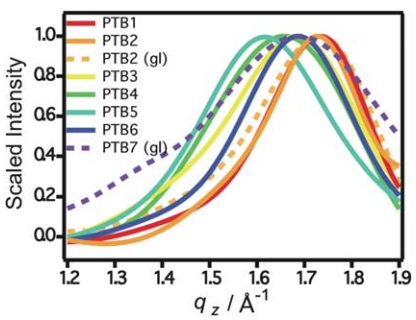

Fig. 5 The π–π stacking scattering vector peaks for seven **PTB** polymers. The solid line shows the scattering peaks for the neat films on a Si substrate while the films on a glass substrate are represented by the dotted lines. (Reproduced from ref. 51.)

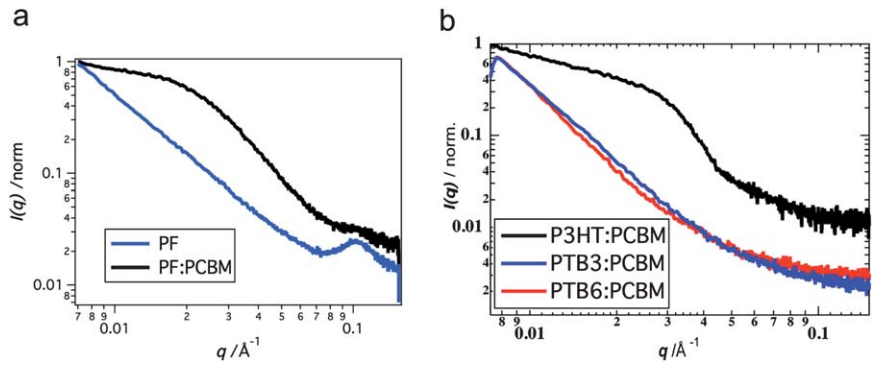

Fig. 6 (a) Horizontal GISAXS line cut of neat and blended **PF** films. The films with **PCBM** show a polydisperse domain 5–10 nm in size, and it is most likely due to **PCBM** islands in the polymer films. From ref. 18. (b)The GISAXS line trace for **PTB6** and **PTB3** blended films. For comparison, the same information for **P3HT**-blended film is shown. (Reproduced from ref. 51.)

X-ray methods, can help to find structural factors at single molecule and molecular assembly levels for enhancing the device PCE. The CS and CR dynamics of the pristine and blended **PF** and **PTB1** films were measured by ultrafast optical transient absorption (TA) spectroscopy with an excitation pump wavelength of 600 nm. The spectral kinetics were monitored using two broad white light continuum light sources ranging from ~500–750 nm in the visible region and ~900–1600 nm in the NIR region. For the **PF** films, the spectral parameters have been described in great detail previously.[18] The TA kinetics and transient spectra of **PF:PCBM** and **PTB1:PCBM** films are shown in Fig. 7. The scaled kinetic traces depicting CS and CR times for both polymers are shown in Fig. 7a while the absorption changes for the polymers are shown in Fig. 7b. For the **PF** films, the spectral parameters have been described in great detail previously.[18] The cation peak formed after CS for both polymers was determined from the visible and NIR spectral results of the neat and blended films. The CS and CR kinetics were monitored at 700 nm, where little change in the absorption upon excitation is observed for neat **PF** films and the presence of the **PF** cation has been established. The **PF:PCBM** film exhibits two time constants for CS: $\tau_{CS1} < 120$ fs (77%) and $\tau_{CS2} = 13.4$ ps (23%). The two constants obtained for CR are $\tau_{CR1} = 406$ ps (13%) and $\tau_{CR2} > 3$ ns (87%).

Similar measurements were performed on the **PTB1** polymer films. The TA spectra in the **PTB1:PCBM** films showed an initial broad exciton absorption at 1320 nm that was quickly depleted, and a new peak at 1150 nm was formed within 0.5 ps of excitation.[35] As was verified previously, the rise of the 1150 nm peak was due to the formation of the cation with a lifetime much longer than a few nanoseconds in the BHJ composite film. Because these two absorption peaks are both broad and overlapping in the NIR region, it becomes difficult to interpret the overall kinetics using the single wavelength transient absorption signals as employed in the **PF** transient absorption analysis. Therefore, the experimental TA spectra of the **PTB1:PCBM** composite films were decomposed into **PTB1** cation and excited exciton absorption spectra. The change in amplitude of the cationic peak with respect to time is the kinetic trace represented in Fig. 7b. The **PTB1:PCBM** film exhibits a biexponential CS dynamics with two time constants of $\tau_{CS1} = 370$ fs (76%) and $\tau_{CS2} = 5.9$ ps (24%) and a biexponential CR dynamics with two constants of $\tau_{CR1} = 931$ ps (30%) and $\tau_{CR2} \geq 2.5$ ns (70%). For the charge separation times, the **PF** showed a faster CS1 time and a slower CS2 time compared to **PTB1**. The first time constant (CS1) is attributed to the crystallinity-dependent charge separation mechanism directly at the donor:acceptor interface. More crystalline domains will exhibit clean interface surfaces, which facilitates CS. The second time constant (CS2) is attributed to the size dependent exciton diffusion in the materials. Therefore, the CS times are consistent with the morphology determined from the GIXS results described previously. In Fig. 7b, it is shown that the cationic peak amplitude is over five times greater for the **PTB1:PCBM** film compared to the **PF:PCBM** film. Although the **PF** kinetic trace is not at the cationic peak maximum, the kinetic spectra in Fig. 7c show a broad, flat spectrum for the cationic peak of **PF**, which indicates that the overall amplitude of the cationic peak is similar in the 700–1000 nm range. Furthermore, the excitonic spectra at early times for the **PTB1:PCBM** and **PF:PCBM** spectra have similar amplitudes, yet the amplitude of the cationic peak at several hundred picoseconds is much smaller for the **PF:PCBM** sample. This finding suggests that the smaller crystal formation significantly enhances the charge separation in the **PTB** polymer films. Although the initial CR time, CR1, is slower for the **PTB1** blended film, the overall amplitude is much higher for this decay compared to **PF** recombination. The larger amplitude of the recombination is rationalized by the increase of the donor:acceptor interface area in the **PTB** polymers while the longer time constant is due to the enhanced roughness of these interfaces. The difference in CR2 could not be determined using the current experimental setup due to the short experimental time window. The larger amplitude of the cationic state is maintained in the **PTB** film after 2 ns, which is also consistent with the higher solar energy conversion of the **PTB** polymer materials. The spectra for the **PF** and the **PTB1** films are shown in Fig. 7c and d, respectively. The transient spectra also confirm the larger amplitude of the cationic state, and therefore the enhancement of charge separation, for the **PTB1** sample. Assuming similar oscillator strengths for the cationic state of the polymer materials, the transient spectra are a direct measure of the relative amount of the cationic species formed in the blended films. The higher generation of separated carriers in the **PTB1** film is explained by the increase of exciton diffusion to the BHJ interfaces. Annealing effects of both materials have also shown that the **PTB** films favor a much smaller domain size compared to **PF** or **P3HT** polymers. Although it has been established that smaller domains are favored in the **PTB** blended films, the mechanisms for this discrepancy, such as the exciton diffusion length and presence of charge transfer states, will be probed in future works.

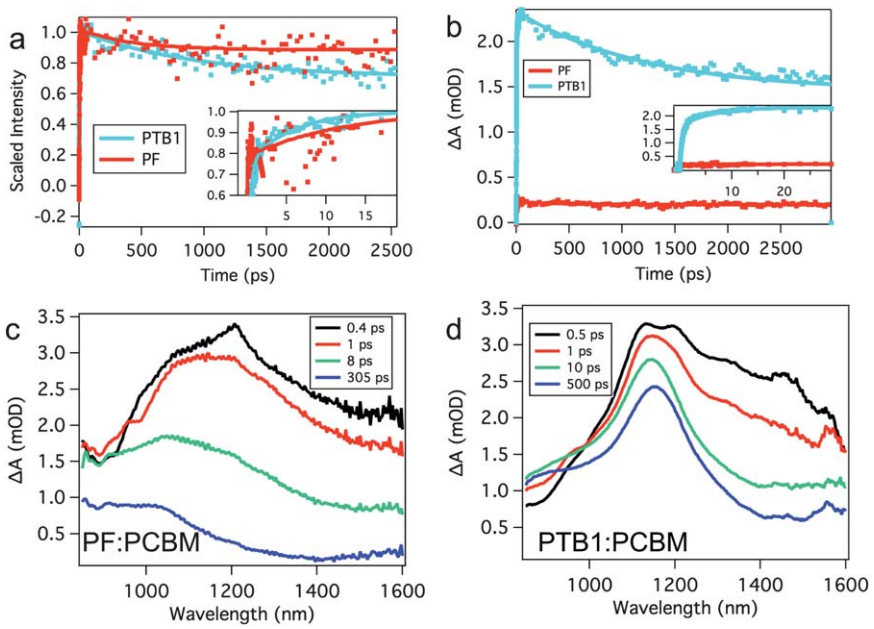

Fig. 7 (a) Scaled and (b) absolute intensity kinetic traces of **PF:PCBM** and **PTB1:PCBM** films. The traces were normalized with respect to the photon absorption of the excitation pulse at 600 nm. The insets in both (a) and (b) are close ups of the kinetic traces at earlier times. (c and d) Transient spectra of (c) **PF:PCBM** and (d) **PTB1:PCBM**. (Reproduced from ref. 18 and 35.)

The electron withdrawing **TT** moiety in the **PF** polymer effectively pulls charge density from adjacent thiophene units, which effectively causes electron density localization. Consequently, the exciton diffusion may be hindered, and the overall PCE of the OPV device may be affected. In **PF**, the **TT** moieties are 6.5 nm apart, so the exciton can become localized on the lower energy segments of the polymer chain. In order to investigate the exciton diffusion of **PF**, in comparison with homocyclic **P3HT**, fluorescence anisotropy measurements were carried out using the fluorescence upconversion. The polarization dependent signals of time-resolved fluorescence for the **PF** and **P3HT** polymers in chlorobenzene are shown in Fig. 8.[52] The measured fluorescence anisotropy decay time constant for **PF** is up to several nanoseconds, which cannot be accurately measured because the **PF** fluorescence lifetime is only 500 ps. What can be determined is that (a) the anisotropy decay can be approximately expressed using one time constant and (b) there is no indication of a fast anisotropy decay component within the instrument response range (300 fs) of this system. The fluorescence anisotropy of the **P3HT** molecule has also been measured both previously[53,54] and in this study as a reference. The fluorescence anisotropy of a conjugated polymer, such as **PF** or **P3HT**, measures the dynamics for the exciton dipole orientational randomization due to exciton hopping or diffusion *via* intrachain and interchain mechanisms. The initial excitation of the polymer is concentrated on a short segment of the entire backbone, followed by the exciton migration through the backbone *via* a Förster type hopping mechanism. The fast fluorescence anisotropy decays observed in **P3HT** are attributed to this hopping mechanism. In the **PF** polymer, however, this rapid exciton dipole orientational randomization due to the exciton hopping was not observed. Therefore, we can deduce that the exciton hopping is relatively slow in **PF**, and hence the dipole orientation would not randomize as fast as those of **P3HT**. This finding implies interplay between the exciton mobility and band gap energy in copolymers. The alternating high and low electron affinity units in the low band gap polymer chain sequence lower the exciton energy and effectively hinder the exciton mobility along the polymer backbone. The effects of the overall PCE on the exciton trapping in **PF** are still ambiguous. Although the exciton mobility of **PF** is lower compared to **P3HT**, the current density of the blended film, which is one of the main indicators of solar cell efficiency, is over 10.2 mA cm^{-2}. This parameter is higher than reported for **P3HT** solar cells with over 5% PCE.[55] The molecular weight of **PCBM** is 910.9 g mol^{-1}, and the diameter of **PCBM** is about 1 nm. Typically polymer/oligomer blends with **PCBM** are optimized at roughly a 1 : 1 weight ratio. If the exciton diffusion length is comparable to the mean distance between **PCBM** acceptor molecules at the polymer/**PCBM** interface, then the hindering exciton migration effect can be minimal. This dependence will be probed further in future works. The anisotropy effects in the **PTB** polymers will also be investigated.

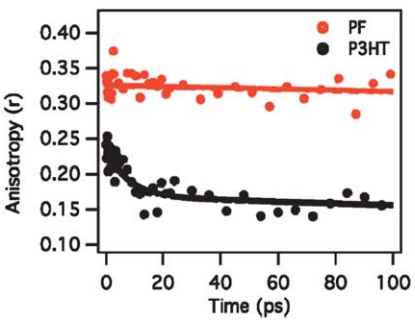

Fig. 8 Measured temporal anisotropy (dots) and anisotropy fits (straight lines) for the **PF** (red) and **P3HT** (black) polymers in chlorobenzene. From ref. 52.

In this report, we have shown that two energetically similar polymer species, **PF** and **PTB**, have drastically different PCEs when blended with **PCBM**. The solar cell morphology in **PTB** is more favorable, which explains the great enhancement in this material. Transient absorption spectroscopy and grazing incidence X-ray studies have verified this claim. We believe that these studies have paved the way to further investigate the interplay between the energetics, morphology, and kinetics in the series of high efficiency low band gap polymers. These polymers are relatively new in the realm of OPV materials. There is still a lot of potential to make these systems even more efficient in order to make OPV devices a viable energy alternative. Various studies on the substrate morphology and carrier generation states are currently underway in our group. We believe that further investigations on these materials will provide very fruitful information on the properties of

these devices, which can be used to push the overall PCE of these materials closer to 10%.

Acknowledgements

This material is based upon work supported as part of the ANSER Center, an Energy Frontier Research Center funded by the U.S. Department of Energy, Office of Science, Office of Basic Energy Sciences under Award Number DE-SC0001059, and is also partially supported by the Division of Chemical Sciences, Office of Basic Energy Sciences, the U.S. Department of Energy under contract DEAC02-06CH11357 (for L.X.C.). We thank Professor Luping Yu and Dr Yongye Liang in the University of Chicago for their discovery and material synthesis of the PF and PTB polymers presented in this highlight. We also thank Drs Joseph W. Strzalka and Byeongdu Lee of the Advanced Photon Source for their help at the beamline setup and useful discussions in data analysis for GIXS, and Dr. David J. Gosztola for his help in using the transient absorption spectroscopy setup at the Center for Nanoscale Materials. The use of the user facilities, the Advanced Photon Source and the Center of Nanoscale Materials in Argonne National Laboratory was supported by the U.S. Department of Energy, Office of Science, Office of Basic Energy Sciences, under Contract No. DEAC02-06CH11357.

References

1 B. A. Bolto, R. McNeill and D. E. Weiss, *Aust. J. Chem.*, 1963, **16**, 1090.
2 C. K. Chiang, C. R. Fincher, Y. W. Park, A. J. Heeger, H. Shirakawa, E. J. Louis, S. C. Gau and A. G. MacDiarmid, *Phys. Rev. Lett.*, 1977, **39**, 1098.
3 C. H. Lee, G. Yu and A. J. Heeger, *Phys. Rev. B: Condens. Matter Mater. Phys.*, 1993, **47**, 15543.
4 F. Wudl, M. Kobayashi and A. J. Heeger, *J. Org. Chem.*, 1984, **49**, 3382.
5 A. Yassar, G. Horowitz, P. Valat, V. Wintgens, M. Hmyene, F. Deloffre, P. Srivasta, P. Lang and F. Garnier, *J. Phys. Chem. C*, 1995, **99**, 9155.
6 Y. Y. Liang and L. P. Yu, *Acc. Chem. Res.*, 2010, **43**, 1227.
7 H. Xin, O. G. Reid, G. Q. Ren, F. S. Kim, D. S. Ginger and S. A. Jenekhe, *ACS Nano*, 2010, **4**, 1861.
8 B. H. Wallikewitz, M. de la Rosa, J. H. W. M. Kremer, D. Hertel and K. Meerholz, *Adv. Mater.*, 2010, **22**, 531.
9 Y. Liang, Z. Xu, J. Xia, S.-T. Tsai, Y. Wu, G. Li, C. Ray and L. Yu, *Adv. Mater.*, 2010, **22**, E135.
10 N. C. Cates, R. Gysel, J. E. P. Dahl, A. Sellinger and M. D. McGehee, *Chem. Mater.*, 2010, **22**, 3543.
11 F. C. Krebs, T. D. Nielsen, J. Fyenbo, M. Wadstrom and M. S. Pedersen, *Energy Environ. Sci.*, 2010, **3**, 512.
12 C. Piliego, T. W. Holcombe, J. D. Douglas, C. H. Woo, P. M. Beaujuge and J. M. J. Frechet, *J. Am. Chem. Soc.*, 2010, **132**, 7595.
13 J. M. Szarko, B. S. Rolczynski, J. Guo, Y. Liang, F. He, M. W. Mara, L. Yu and L. X. Chen, *J. Phys. Chem. B*, 2010, **114**, 14505.
14 L. S. Hung and C. H. Chen, *Mater. Sci. Eng., R*, 2002, **39**, 143.
15 G. Dennler, M. C. Scharber and C. J. Brabec, *Adv. Mater.*, 2009, **21**, 1323.
16 F. C. Krebs, J. Fyenbo and M. Jorgensen, *J. Mater. Chem.*, 2010, **20**, 8994.
17 E. Bundgaard and F. Krebs, *Sol. Energy Mater. Sol. Cells*, 2007, **91**, 954.
18 Y. Y. Liang, D. Q. Feng, J. C. Guo, J. M. Szarko, C. Ray, L. X. Chen and L. P. Yu, *Macromolecules*, 2009, **42**, 1091.
19 Y. Liang, S. Xiao, D. Feng and L. Yu, *J. Phys. Chem. C*, 2008, **112**, 7866.
20 Y. Y. Liang, Y. Wu, D. Q. Feng, S. T. Tsai, H. J. Son, G. Li and L. P. Yu, *J. Am. Chem. Soc.*, 2009, **131**, 56.
21 Y. Y. Liang, D. Q. Feng, Y. Wu, S. T. Tsai, G. Li, C. Ray and L. P. Yu, *J. Am. Chem. Soc.*, 2009, **131**, 7792.
22 Y. Yao, Y. Liang, V. Shrotriya, S. Xiao, L. Yu and Y. Yang, *Adv. Mater.*, 2007, **19**, 3979.
23 Y. Y. Liang and L. P. Yu, *Polym. Rev.*, 2010, **50**, 454.
24 C. J. Brabec, N. S. Sariciftci and J. C. Hummelen, *Adv. Funct. Mater.*, 2001, **11**, 15.
25 E. Bundgaard, O. Hagemann, M. Manceau, M. Jorgensen and F. C. Krebs, *Macromolecules*, 2010, **43**, 8115.
26 C. Y. Li, T. C. Wen, T. H. Lee, T. F. Guo, J. C. A. Huang, Y. C. Lin and Y. J. Hsu, *J. Mater. Chem.*, 2009, **19**, 1643.
27 M. Sommer, S. Huettner and M. Thelakkat, *J. Mater. Chem.*, 2010, **20**, 10788.
28 M. Sommer, S. Huettner and M. Thelakkat, *Adv. Polym. Sci.*, 2010, **228**, 123.
29 M. D. Irwin, B. Buchholz, A. W. Hains, R. P. H. Chang and T. J. Marks, *Proc. Natl. Acad. Sci. U. S. A.*, 2008, **105**, 2783.
30 J. L. Bredas, D. Beljonne, V. Coropceanu and J. Cornil, *Chem. Rev.*, 2004, **104**, 4971.
31 F. G. Brunetti, R. Kumar and F. Wudl, *J. Mater. Chem.*, 2010, **20**, 2934.
32 M. Scharber, D. Mühlbacher, M. Koppe, P. Denk, C. Waldauf, A. Heeger and C. Brabec, *Adv. Mater.*, 2006, **18**, 789.
33 J. Y. Kim, S. H. Kim, H. H. Lee, K. Lee, W. L. Ma, X. Gong and A. J. Heeger, *Adv. Mater.*, 2006, **18**, 572.
34 I. F. Perepichka, D. F. Perepichka, H. Meng and F. Wudl, *Adv. Mater.*, 2005, **17**, 2281.
35 J. C. Guo, Y. Y. Liang, J. Szarko, B. Lee, H. J. Son, B. S. Rolczynski, L. P. Yu and L. X. Chen, *J. Phys. Chem. B*, 2010, **114**, 742.
36 M. Y. Chiu, U. S. Jeng, C. H. Su, K. S. Liang and K. H. Wei, *Adv. Mater.*, 2008, **20**, 2573.
37 H. H. Yang, S. W. LeFevre, C. Y. Ryu and Z. Bao, *Appl. Phys. Lett.*, 2007, **90**, 172116.
38 S. K. Hau, H. L. Yip, O. Acton, N. S. Baek, H. Ma and A. K. Y. Jen, *J. Mater. Chem.*, 2008, **18**, 5113.
39 S. Miller, G. Fanchini, Y. Y. Lin, C. Li, C. W. Chen, W. F. Su and M. Chhowalla, *J. Mater. Chem.*, 2008, **18**, 306.
40 L. G. Li, G. H. Lu and X. N. Yang, *J. Mater. Chem.*, 2008, **18**, 1984.
41 M. Drees, H. Hoppe, C. Winder, H. Neugebauer, N. S. Sariciftci, W. Schwinger, F. Schaffler, C. Topf, M. C. Scharber, Z. G. Zhu and R. Gaudiana, *J. Mater. Chem.*, 2005, **15**, 5158.
42 G. Li, V. Shrotriya, Y. Yao, J. S. Huang and Y. Yang, *J. Mater. Chem.*, 2007, **17**, 3126.
43 B. S. Rolczynski, J. M. Szarko, B. Lee, J. Strzalka, J. C. Guo, Y. Y. Liang, L. P. Yu and L. X. Chem, *J. Mater. Res.*, 2011, **26**, 296.
44 H. Sirringhaus, P. J. Brown, R. H. Friend, M. M. Nielsen, K. Bechgaard, B. M. W. Langeveld-Voss, A. J. H. Spiering, R. A. J. Janssen, E. W. Meijer, P. Herwig and D. M. de Leeuw, *Nature*, 1999, **401**, 685.
45 Y. Fang, S. A. Chen and M. L. Chu, *Synth. Met.*, 1992, **52**, 261.
46 Y. J. Cheng, C. H. Hsieh, Y. J. He, C. S. Hsu and Y. F. Li, *J. Am. Chem. Soc.*, 2010, **132**, 17381.
47 M. Reyes-Reyes, K. Kim, J. Dewald, R. Lopez-Sandoval, A. Avadhanula, S. Curran and D. L. Carroll, *Org. Lett.*, 2005, **7**, 5749.
48 N. C. Cates, R. Gysel, Z. Beiley, C. E. Miller, M. F. Toney, M. Heeney, I. McCulloch and M. D. McGehee, *Nano Lett.*, 2009, **9**, 4153.
49 X. N. Yang, J. Loos, S. C. Veenstra, W. J. H. Verhees, M. M. Wienk, J. M. Kroon, M. A. J. Michels and R. A. J. Janssen, *Nano Lett.*, 2005, **5**, 579.
50 H. Hoppe and N. S. Sariciftci, *J. Mater. Chem.*, 2006, **16**, 45.
51 J. M. Szarko, J. C. Guo, Y. Y. Liang, B. Lee, B. S. Rolczynski, J. Strzalka, T. Xu, S. Loser, T. J. Marks, L. P. Yu and L. X. Chen, *Adv. Mater.*, 2010, **22**, 5468.
52 J. M. Szarko, B. S. Rolczynski, J. Guo, Y. Liang, F. He, M. W. Mara, L. Yu and L. X. Chen, *J. Phys. Chem. B*, 2010, **114**, 14505.
53 S. Westenhoff, C. Daniel, R. H. Friend, C. Silva, V. Sundstrom and A. Yartsev, *J. Chem. Phys.*, 2005, **122**, 094903.
54 N. P. Wells, B. W. Boudouris, M. A. Hillmyer and D. A. Blank, *J. Phys. Chem. C*, 2007, **111**, 15404.
55 M. Reyes-Reyes, K. Kim and D. L. Carroll, *Appl. Phys. Lett.*, 2005, **87**, 083506.